Linear and Star Branched Perylene-Containing Polyimides: Synthesis, Characterization, and Photovoltaic Properties of Novel Donor–Acceptor Dyes Used in Solar Cell

Haijun Niu,[1,2] Jun Luo,[1] Wenjun Wu,[2] Jingshan Mu,[1] Cheng Wang,[1] Xuduo Bai,[1] Wen Wang[3]

[1]*Key Laboratory of Functional Inorganic Material Chemistry (Heilongjiang University), Ministry of Education, Key laboratory macromolecular chemistry, Harbin 150080, People's Republic of China*
[2]*Key Laboratory for Advanced Materials and Institute of Fine Chemicals, East China University of Science and Technology, Shanghai 200237, People's Republic of China*
[3]*School of Material Science and Engineering, Harbin Institute of Technology, Harbin 150080, People's Republic of China*

Received 17 May 2011; accepted 7 August 2011
DOI 10.1002/app.35458
Published online 17 December 2011 in Wiley Online Library (wileyonlinelibrary.com).

ABSTRACT: A series of novel linear and star branched triphenylamine-containing aromatic polyimides (AI, AII, AIII) were designed and synthesized by the condensation of 4-aminotriphenylamine(I), 4,4′-diamino triphenylamine(II), 4,4′,4″-triamino triphenyl-amine(III) with perylene-3,4,9,10-tetra-carboxylic dianhydride to investigate the influence of topological structure on the energy levels and photophysical performance. The polyimides were characterized by elemental analysis, FTIR, and ^{1}H-NMR. The onset temperatures for 5% weight loss determined by thermoanalysis were between 415 and 428°C. The results of UV–vis spectra, quantum chemical calculation, and cyclic voltammetry revealed that introduction of triphenylamine group changed the energy levels of entire dye system. The aggregation way of polymers was also studied by the methods of UV–vis spectra, X-ray diffraction (XRD), atom force microscopy, and the molecular simulation. The dye-sensitized solar cells prepared by using the series of dyes showed big photoelectric response. © 2011 Wiley Periodicals, Inc. J Appl Polym Sci 125: 200–211, 2012

Key words: perylene diimide; triphenylamine; sensitized solar cell; electrochemistry; optical properties

INTRODUCTION

Dye-sensitized solar cells' Grätzel cells (DSSCs) have attracted a great deal of interest, as they offer high energy-conversion efficiencies at low cost. Ruthenium dyes are used in DSSCs containing titania nanocrystals, exhibit high performance and good stability with record solar energy-to-electricity conversion efficiency of 11% under AM 1.5 irradiation.[1] Because of the use of rare metals and the difficulty of purification, the organic and conducting polymers offer the prospective of very low cost fabrication and present attractive features that facilitate market entry.

Recently, organic dyes have received more and more attention for their structure variety, high molar extinction coefficients, and simple preparation process of low cost in comparison to ruthenium complexes. Metal-free dyes such as perylene dyes,[2] cyanine dyes,[3] merocyanine dyes,[4] coumarin dyes,[5] porphyrin dyes,[6] and indoline dyes[7] have been investigated as sensitizers for DSSCs, yielding respectable conversion efficiencies between 5 and 9% with the traditional iodide/triiodide redox.

Perylene diimides are important electron acceptors and electron-transporting materials that have been used in high-tech applications, spanning from electronic to biological fields, such as optical switches, lasers, deoxyribonucleic acid/ribonucleic acid (DNA/RNA) probes, and so on.[8–10] It is well known that the perylenetetracarboxylic acid is easy to form close π–π aggregation that can not only lead to self-quenching and reduction of electron injection into TiO_2 but also to the instability of the organic dyes due to the formation of excited triplet states and unstable radicals under light irradiation. However, this shortcoming may be overcomed by chemical modifications. Sensitizers derived from perylene imides have also received much attention due to their outstandingly

Additional Supporting Information may be found in the online version of this article.

Correspondence to: H. Niu (haijunniu@hotmail.com) and X. Bai (xuduobai@hotmail.com).

Contract grant sponsor: National Science Foundation of China; contract grant numbers: 21074031, 50872024, 20872030.
Contract grant sponsor: Heilongjiang University Outstanding Youth Science Foundation.
Contract grant sponsor: Heilongjiang University Innovator Group; contract grant number: hdtd-2010-11.
Contract grant sponsor: Foundation of Heilongjiang Education Bureau; contract grant number: 12511379.

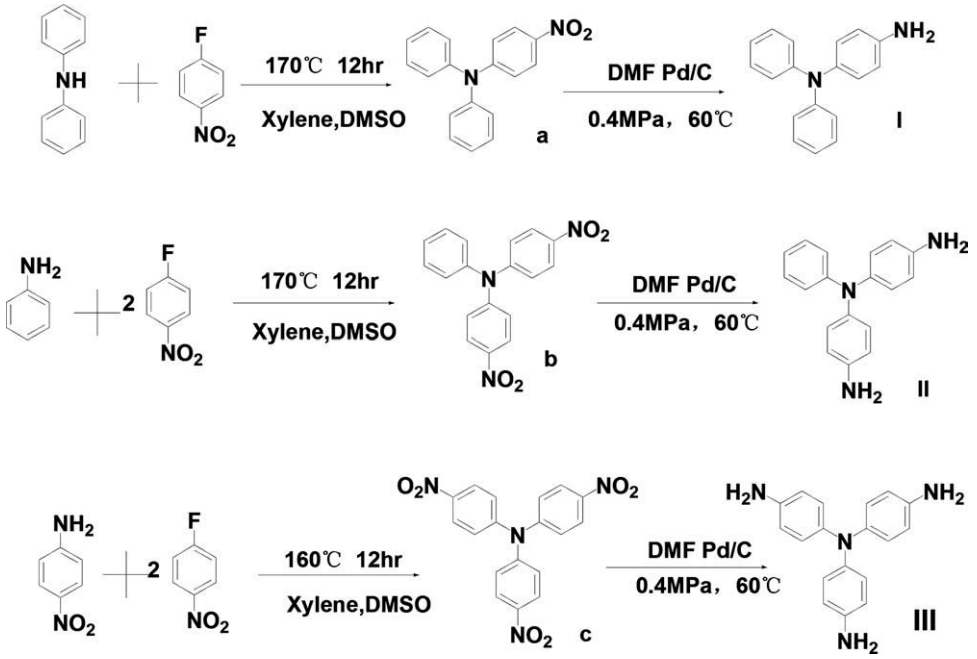

Figure 1 Synthesis route for monomers: I, II, and III.

chemical, thermal, and photochemical stabilities and high molar extinction coefficient in the visible to NIR range.[11–19] Up to now, a record of photoconversion efficiency of 2.6% has been reported by Imahori and coworkers[20] with dipyrrolidinyl perylene bisimide derivatives, and the overall solar to electrical energy conversion efficiency was improved to almost 4% for the dye with intramolecular charge transfer character, but in the latter dye, there was C—N bond instead of imide bond between the donor and acceptor.[21]

Recently, it has been found that by incorporating electron donor triarylamine group into the dye molecules, the physical separation of the dye cation from the electrode surface will be increased, which fascinates to achieve high rates of charge separation and collection compared with interfacial charge-recombination processes, and many higher efficient DSSCs based on the concept have been built.[22–25] In order to improve the solubility of the imide and to enlarge intramolecular charge separation, we have designed, synthesized the novel organic and polymeric sensitizers: AI, AII, AIII that consist of the triarylamine moiety acting as electron donor (D) and perylene acid moiety acting as acceptor (A) and investigated the influence of D-A-D, D-A types of structures on the optical, electrochemical, energy levels, photovoltaic properties, and morphologies.

EXPERIMENTAL

Materials

3,4,9,10-Perylenetetracarboxylic acid dianhydride (PTDA) and isoquinoline were purchased from Aldrich. Ferrocene and tetrabutylammonium perchlorate were purchased from Acros and used for the electrochemical characterization of polymers. *N*,*N*-dimethylformamide, *N*-methyl-2-pyrrolidinone (NMP), dimethyl sulfoxide (DMSO), *m*-cresol, and other reagents were reagent grade and used as received unless otherwise stated. Cis-di(thiocyanato)-*N*,*N*′-bis (2,2′-bipyridyl-4-carboxylic acid-4′-tetrabutyl ammonium carboxylate) ruthenium(II) was the commercial product by the trade name of N719 obtained from Solaronix S.A., Aubonne, Switzerland.

Typical procedure for the monomer synthesis

The monomers based on triphenylamine were synthesized in according to Figure 1. A total of 20.84 g (0.072 mol) of the desired nitro compound such as 4-nitro-triphenylamine and 0.4 g of Pd/C (10 wt % palladium on activated carbon) were charged into a pressure reactor and reacted for 72 h at 200 rpm under 0.4 MPa of hydrogen pressure. Catalyst was removed by filtration over celite, followed by solvent evaporation and recrystallization from ethanol under nitrogen, white needles was obtained (15.89 g, 85% yield). Other two triphenylamines were prepared by an analogous procedure according to Figure 1.

Compound I: yield: 85%; m.p. = 148∼ 150°C; IR (KBr, cm^{-1}): 3430, 3350 (*N*—H asymmetric and symmetric stretching). 3036 (aromatic C—H stretching), 1624, 1584 (*N*—H bending and aromatic ring stretching), 1509, 1403(aromatic ring stretching), 1330, 1269 (C—N stretching), 1220, 829 (C—H bending in 1,4 substituted ring), 754, 695 (C—H bending in single substituted ring). ^{1}H-NMR (DMSO-d_6, ppm): 6.47 (d,

2H), 6.80 (d, 4H), 7.09 (t, 4H), 6.67∼ 6.72 (m, 4H), 4.94 (s, 2H, NH). Anal. Calcd. for $C_{18}H_{16}N_2$ (260.33): C, 83.04%; H, 6.19%; N, 10.76%. Found: C, 83.35%; H, 6.19%; N, 10.72%.

Compound II: yield: 81%; m.p. = 191°C; IR (KBr, cm^{-1}): 3430, 3340 (*N*—H asymmetric and symmetric stretching), 3030 (aromatic C—H stretching), 1623, 1590 (*N*—H bending and aromatic ring stretching), 1500, 1403 (aromatic ring stretching), 1330, 1280 (C—N stretching), 827 (C—H bending in 1,4-substituted ring), 761, 696 (C—H bending in single substituted ring). ^{1}H-NMR (DMSO-d_6, ppm): 6.94 (dd, 2H), 6.75∼ 6.60 (m, 4H), 6.60∼ 6.33 (m, 7H), 4.85 (s, 4H); Anal. calcd for $C_{18}H_{17}N_3$ (260.36): C 78.52%, H 6.22, N 15.26%; found C 78.65%, H 6.32%, N 15.36%.

Compound III: yield: 89%; m.p. = 246°C; IR (KBr, cm^{-1}): 3406, 3336 (*N*—H asymmetric and symmetric stretching), 3029 (aromatic C—H stretching), 1618 (*N*—H bending and aromatic ring stretching), 1502, 1405 (aromatic ring stretching), 1331, 1261 (C—N stretching), 829 (C—H bending in 1,4-substituted ring). ^{1}H-NMR (DMSO-d_6, ppm): 6.35 (6H, ArH), 6.31 (6H, ArH), 4.52 (6H, ArH). Anal. Calcd. for $C_{18}H_{16}N_2$ (290.40): C, 83.04%; H, 6.19%; N, 10.76%. Found: C, 83.35%; H, 6.19%; N, 10.72%.

Typical procedure for the syntheses of imides and polyimides

In a three-necked, round-bottomed flask fitted with an Ar inlet/outlet and a Dean-Stark trap, PTDA (0.3923 g, 1 mmol), amine I (0.5206 g, 2 mmol), and 2 mL of isoquinoline were dissolved in 60 mL of *m*-cresol. The reaction solution was heated to 200°C for 24 h, and during the course of the reaction, about 15 mL of *m*-cresol was distilled off. The mixture was then cooled to 100°C and poured into 300 mL of methanol. The precipitated polymer was collected by filtration and washed with methanol several times. Unreacted PTDA was removed by treatment with 10% sodium hydroxide several times, until the green fluorescent color in basic solution faded away. The crude product was treated with acetone in a Soxhlet apparatus for 24 h, to remove high boiling point solvents such as *m*-cresol and isoquinoline. The dark brown precipitate was collected and dried at 80°C under vacuum (0.6846 g, 75% yield). AII and AIII were prepared by the same method to that of AI shown in Figure 2, except that the raw materials mol ratios of PTDA to triphenylamine are 1 : 1 of AII and 2 : 3 of AIII, respectively.

AI: yield 75%; IR (KBr, cm^{-1}): 1716, 1658 (imide stretch). ^{1}H-NMR (DMSO-d_6, δ, ppm): 8.22 (PTDA-H), 7.34∼ 6.77 (ArH). Anal. Calcd. for ($C_{60}H_{36}N_4O_4$) 876.97: C, 82.17%; H, 4.15%; N, 6.39%. Found: C, 77.87%; H, 3.76%; N, 5.04%.

AII: Yield: 80%; IR (KBr, cm^{-1}): 1717, 1658 (imide stretch). ^{1}H-NMR (DMSO-d_6, δ, ppm): 8.35 (PTDA-H), 7.28∼ 6.62 (ArH). Anal. Calcd. for ($C_{42}H_{21}N_3O_4$) 631.66: C, 79.87%; H, 3.35%; N, 6.65%. Found: C, 75.49%; H, 3.15%; N, 5.21%.

AIII: Yield: 82%; IR (KBr, cm^{-1}): 1714, 1657 (imide stretch). Anal. Calcd. for ($C_{108}H_{48}N_8O_{12}$) 1649.57: C, 78.63%; H, 2.94%; N, 6.79%. Found: C, 74.14%; H, 4.10%; N, 5.55%.

Fabrication of DSSCs

DSSCs were fabricated using fluorine-doped tin oxide (FTO) glass (20∼ 25 Ω^2 Nippon glass) as substrates for both photoelectode and counter electrode. For the preparation of photoeletrode, a mesoporous film of anatase TiO_2 coated on the FTO glass substrate was fabricated by sol–gel process according to the literature.[24] In general, in a modified sol–gel synthesis, two solutions were prepared. A Ti-precursor solution (namely solution A) was formed via adding 10 mL tetrabutyl titanate and 1.5 mL acetylacetone to 10 mL absolute ethanol. A mixture of 0.2 mL hydrochloric acid, 2 mL double distilled water, and 4 mL absolute ethanol (namely solution B) was added dropwise into the solution A under ultrasonic, and the viscosity of the solution increased gradually with hydrolytic reaction proceeding. At last, a bright yellow and transparent sol (Meso-TiO_2 sol) was obtained after 1 h reaction. Meso-TiO_2 sol was spread on FTO glass by dipping method and then was calcinated at 380°C for 30 min in air. Then TiO_2 paste (P25 paste, Degussa) was deposited onto substrate mentioned above. After TiO_2 being dried, the covered glass plates were sintered in air for 30 min at 450°C, cooled to about 80°C, and immersed in anhydrous *m*-cresol containing dyes for 48 h at room temperature; excess dye was removed by rinsing with *m*-cresol, acetonitrile and dried in vacuum at 80°C. The thickness of the TiO_2 was about 16 μm determined by profiler. The N719-sensitized electrode was made in similar way for reference. The FTO counter electrode was thermally platinized by depositing 15 μL of 5 m*M* H_2PtCl_6 in 2-propanol and heated to 380°C for 15 min. The assembly of DSSCs was done by pressing the counter-electrode against the coated dye-sensitized electrode spaced with a 60 μm Surlyn-1760 frame, and then the electrolyte was introduced from the edge of the two glass substrates just before measurements. The surface area of the TiO_2 film electrode under illumination was 0.25 cm^2. The electrolyte was 0.6*M* 1-butyl-3-methylimidazolium iodide (BMII), 0.1*M* LiI, 0.05*M* I_2 solution in acetonitrile with 0.5*M* 4-tertbutyl-pyridene (4-TBP).

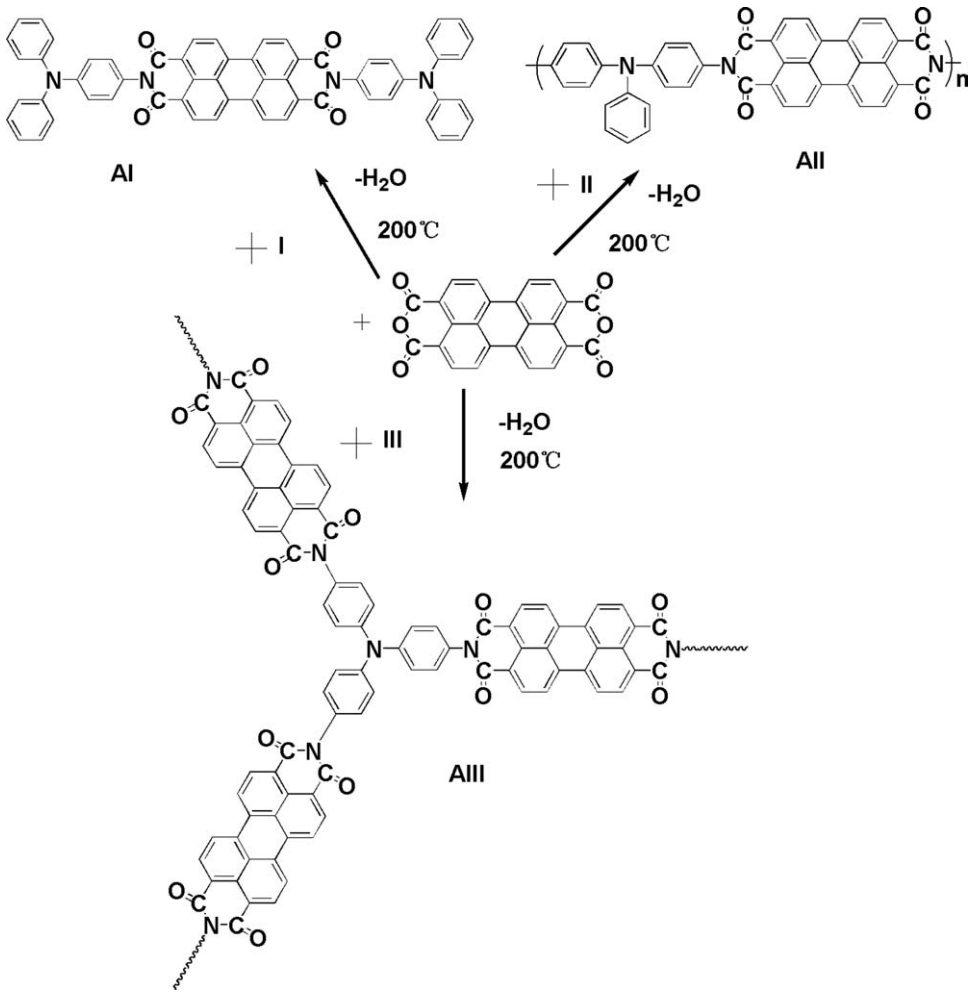

Figure 2 Synthesis route for model compounds and polymers: AI, AII, and AIII.

Instruments and characterization

^{1}H-NMR spectra were recorded on a Bruker-300 instrument using tetramethylsilane as an internal reference. Infrared measurements were performed on a PE FTIR spectrometer. UV–vis absorption spectra of the dyes in solution and adsorbed on TiO_2 were measured on SHIMADZU UV-1700 spectrophotometer. Photoluminescence spectra were measured on Jasco FP-6200 spectrophotometer. The emission spectra of dyes were taken at $\lambda_{exc} = 520$ nm. Melting points were obtained with a WRX-4 microscopy apparatus that were uncorrected. Inherent viscosities were measured in concentrated H_2SO_4 solution at 25 ± 0.1°C using an Ubbelohde dilution viscometer. The stabilities and glass-transition temperatures (T_gs) of the polymer samples were determined using a NETGSCH49C at a heating rate of 10°C/min under nitrogen flow (50 mL/min). X-ray diffraction patterns were recorded using powder samples on a wide-angle D/max-γB diffractometer working in typical Bragg geometry with Cu Kα radiation. The morphology observation of the samples was carried out on a field-emission scanning electron microscopy (Mx2600fe) and atom force microscopy (AFM, Nanoscope IIIa digital instrument) equipped with a silicon cantilever (typical spring constant 40 Nm^{-1}) in tapping mode under ambient conditions.

Electrochemical measurements were performed on a CHI660 electrochemical analyzer to obtain all $E^o_{1/2}$s via cyclic voltammograms (CV) calibrated to Fc(II)/Fc(III) oxidation couple. CV experiments were carried out in three-electrode cell consisting of a platinum working electrode, a platinum counter electrode and a Ag/Ag^+ reference electrode. Solutions of the polyimides and compounds were prepared in reagent grade NMP dried over 4-Å molecular sieves. The supporting electrolyte was 0.1*M* tetra-*n*-butylammonium perchlorate dried overnight at 100°C. The solution was deoxygenated by sparging with Ar for 15 min prior to scanning and was blanketed with Ar during scans. CV was performed with microelectrode technique according to the literature.[26]

Photocurrent-voltage characteristics of solar cells and photocurrent action spectra (incident photon-to-photocurrent efficiency, IPCE) for the polymer-modified electrodes were obtained with CHI instrument under simulated light source using a 500W high-pressure Xe lamp as the excitation light source, with the collimated light beam passing through an grating monochromator (Tianjin Lanlik) to select the excitation wavelength when the steady-state photocurrent was recorded. The incident light intensities at the different wavelengths were measured with a Light Radiometer (Beijing Normal University).

Density functional theory (DFT) calculations were performed on a computer. Geometry optimizations were carried out using the B3LYP functional and 6-31G basis set, as implemented in Gaussian 98 program.[27] Molecular dynamics(MD) simulations were carried out using MATERIALS Studio software package (Accelrys). The models were built with a Visualizer module, the molecular dynamics, and the minimization calculations were performed on the Discover module. The force field, we implemented in this work, was condensed-phase optimized molecular potentials for atomistic simulation studies (COMPASS), which was based on the earlier class II CFF9x and PCFF force fields and was the first *ab initio*-based force field that was parameterized using extensive data for molecules in the condensed phase. The MD simulations were performed within a canonical ensemble (NVT) at 298 K, and the temperature was controlled by Andersen method. The smart minimizer was used, combining the steepest descents method and conjugate gradient method.

RESULTS AND DISCUSSION

Monomer and polymer synthesis

4-Aminotriphenylamine(I), 4,4′-diaminotriphenylamine(II), and 4,4′,4″-triamino triphenyl-amine(III) were prepared by the condensation of diphenylamine, aniline, 4-nitroaniline with 1-fluoro-4-nitrobenzene followed by hydrazine Pd/C catalytic reduction according to the synthetic route outlined in Figure 1. The monomers successfully synthesized were identified by elemental analysis, IR, and ^{1}H-NMR spectroscopic techniques in agreement with the literatures.[28–30] The nitro groups of compounds a, b, c that gave two characteristic bands at 1580 and 1313 cm^{-1} ($-NO_2$ asymmetric and symmetric stretching) disappeared after the reduction, and the amino group showed the typical *N*—H stretching absorption pair in the region of 3300∼ 3500 cm^{-1}. The ^{1}H-NMR spectra of compounds a, b, c confirmed that the nitro groups have been completely transformed into amino groups by the high-field shift of the aromatic protons and by the resonance signals at around 4.5 ppm corresponding to the amino protons.

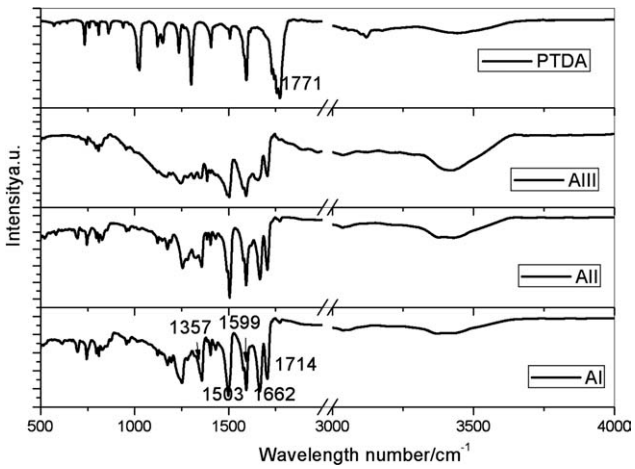

Figure 3 IR spectra of compounds and polymers AI, AII, and AIII.

Reaction of monoamine(I), diamine(II), and triamine (III) with dianhydrides (PTDA) with the reaction ratio of 2 : 1, 1 : 1, and 2 : 3 was carried out at 200°C in refluxing *m*-cresol containing a small amount of isoquinoline by one-step method according to the Figure 2. AII, AIII were obtained in high yield with intrinsic viscosities in range of about 0.4 dL/g in concentrated sulfuric acid in agreement with the literatures.[19,31] Owing to the low solubility of PTDA in *m*-cresol at room temperature, higher temperature may increase its solubility. The generated water was removed through a gentle argon flow, and hence, the reaction equilibrium was moved to the formation of polyimide. Because the polymers were partly soluble in common organic solvents, their molecular weights could not be obtained.

The reaction mixture slowly dissolved on imidization to give a deep red solution and the product precipitated upon cooling to 100°C. The ^{1}H-NMR spectra of perylene imides showed multiplet resonances at about 8.2 (8.7) representing the aromatic protons from the perylene moiety, other resonances at about 7.2 representing the aromatic protons from triphenylamine. Complete imidization was confirmed by IR spectroscopy, which indicated the loss of six-membered anhydride peaks at 1773, 1756 cm^{-1} and the appearance of the characteristic imide peaks at 1716, 1668 cm^{-1}(Fig. 3). The reaction procedure also can be monitored by IR. When some raw materials existed, there were peaks at 1773, 1756 cm^{-1} in IR spectra. The raw product was washed with 10% sodium hydroxide solution to discard unreacted materials. In all cases, however, the carbon and nitrogen elemental analysis values were lower than the calculated values in the proposed structures. This probably relates to higher char yields of these polymers

TABLE I
The Heat Stability Analysis of AI, AII, AIII

	TB_g (°C)$_B$	5% Mass (°C)	10% Mass (°C)	Residual % (700°C)
A_I	–	425	483	52
A_{II}	248	425	515	46
A_{III}	268	418	470	60

at elevated temperatures, which will be discussed subsequently.

Thermal properties and crystalline

All polyimides and model compounds synthesized were characterized by differential scanning calorimeter (DSC) and thermogravimetry (TG). The results were summarized in Table I. As indicated by the onset temperatures of decomposition (T_d) for 5% weight loss ranging from 418 to 425°C (Supporting Information Fig. S1), polyimides were quite thermally stable in nitrogen. The amount of carbonized residue (char yield) of these PTDA-containing polymers in nitrogen atmosphere was more than 46% at 700°C. The T_gs of all the polymers were observed in the range of 248∼ 268°C. This result also supports the amorphous nature of these triphenylamine-containing polymers, which showing no peak of T_m. The polydispersity maybe so wide that the polyimide experience phase transition during a large temperature range and the molecular chain is so stiff that the molecule can move at higher temperature.

To investigate the aggregation state in the compounds, the XRD patterns of model compounds and polyimides powders were obtained and shown in Supporting Information Figure S2. Broad diffraction peaks of diffusion type centered at 23° (2θ) were observed in plots. The steric repulsion of the bulky triphenylamine unit twists the rings dramatically out of the plane, which inhibits chain packing and crystallization. The pristine polyimides and model compound are amorphous. The results are in line with the results of DSC determination. All perylene-containing dyes are soluble in polar aprotic solvents such as NMP, concentrated sulfuric acid, *m*-cresol, and stable at room temperature. The polyimides exhibit solubility because of the increased flexibility and free volume caused by the introduction of a bulky pendent triphenylamine group in the repeat unit.

Morphologies of films

Supporting Information Figure S3 shows the tapping-mode AFM topographical images (1×1 μm^2) of the polyimides films. The films were casted from *m*-cresol and annealed at 120°C to make the solvent evaporate. The coatings were homogenous and porous. The films of AII and AIII were rough (mean roughness, Ra = 7.73 nm and 7.85 nm), which could make ion of electrolyte penetrate readily and would improve the current in the solar cell.

Optical properties

The UV–vis spectra obtained in different polar solvent such as DMSO, NMP, *m*-cresol, concentrated H_2SO_4 were summarized in Supporting Information Table S1. As shown in Figure 4, in DMSO, the AI spectrum showed the characteristic four modal absorbance peaks at 432, 460, 493, 528 nm, which attributed to 0→ 3, 0→ 2, 0→ 1, 0→ 0 transition. The peaks of three dyes were in the similar place and shifted to low energy region by 6 or 13 nm compared with PTDA. This implies the linear and star structures play minor role in the UV–vis spectrum compared with model compound. The absorption and fluorescence spectra of compounds showed consistent mirror-image behavior as shown in reference.[32]

However, in strong polar solvent, such as *m*-cresol, the peaks of AI moved to low energy region by about 24 nm compared with that in DMSO. As shown in the spectrum in H_2SO_4, besides that the peaks moved to long wavelength, a new peak appeared in 600 nm, which may be explained by interaction of the dye with H_2SO_4 and protonation of dyes.[31,33] The perylene pigments we synthesized were dissolved in concentrated sulfuric acid and reobtained by dilution showing no decomposition. So, we think the concentrated sulfuric acid was not easy to destroy the molecule. The new peak was mainly attributed to the interaction of concentrated sulfuric and perylene pigments.

We also investigated the peaks position dependence of concentration and found that no new peak appeared (representing dimer or aggregation) with the increasing of concentration of dyes. When the dyes were absorbed by TiO_2, the absorption peaks did not blue shift like the ref. 24. There only plots of absorption superimposed over the spectra of dyes in solvent. The absorbance of the thin film was governed by the monomer like that in dilution. This did not indicate that H- or J-aggregation formed in concentrated solution or in films, which would quench the photogenerated electron, induce to recombination of electrons and holes, thus decrease the photocurrent density. This can be explained by the introduction of nonplanar triphenylamine moiety, which gave hindrance of aggregation. This will be discussed by molecular simulation in the next section.

Electrochemical properties

CV was used to determine the redox potentials of the dyes and to estimate the driving force of the

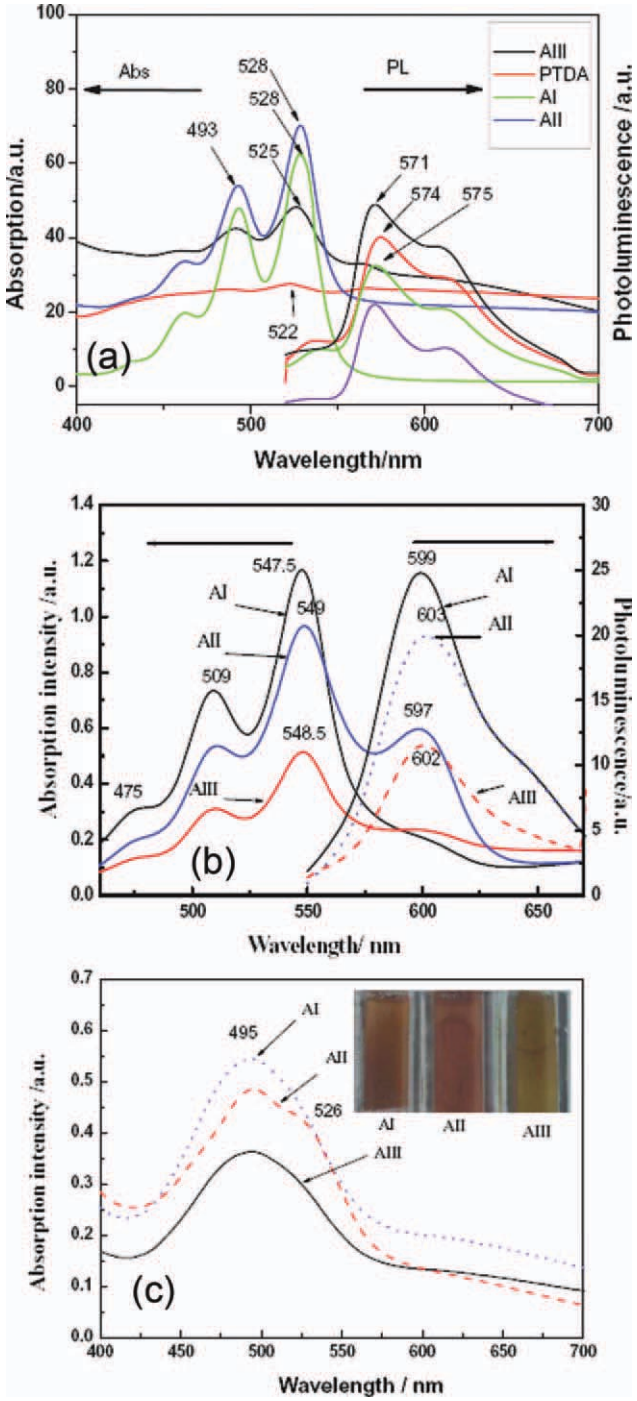

Figure 4 UV–vis spectra of AI, AII, and AIII (a) in DMSO; (b) in concentrated H_2SO_4; (c) on TiO_2 nanofilms. [Color figure can be viewed in the online issue, which is available at wileyonlinelibrary.com.]

photoinduced electron injection process. The CV curves of a series of compounds were shown in Figure 5. able II summarized E_{LUMO}s calculated from the redox half-wave potentials in CV and band gaps (E_g^{opt}) estimated from the onset absorption wavelength of maximum absorption wavelength (λ_{max}), assuming that the HOMO energy level for the Fc/Fc^+ standard was 4.80 eV with respect to the zero vacuum level. The measured E_{LUMO}s and calculated E_{HOMO}s were listed in Table II, respectively, which suggested that the three types of triphenylamine derivatives exhibited analogous energy levels.

For example, AI underwent two reversible one-electron reductions. The first of which was the reduction of the neutral monomer to the radical anion and the second reduction corresponded to the formation of the dianion. The others dyes behave similarly. However, during the anodic scan, no strikingly reversible oxidations of compounds representing the characteristic of triphenylamine were observed. It implied perylene cores that had the characteristic of the intensive withdrawing electron played the key role.

Despite different chemical structures, it was mainly the conjugated planar structure that determined the energy levels as well as the band gaps other than alkyl group.[15] The results from CV measurements illustrated that the compounds could be easily reduced (*n*-doped), which implied that the polymers possessing the capability for accepting electron were *n*-type semiconductors. The energy levels of the HOMO were lower for the compounds compared with the redox potential of I^-_3/I^- (−5.03 eV, referring to vacuum), which meant that the dyes had more driving force to be reduced by the I^-_3/I^- redox system in thermodynamics due to the shift in ionization potential. The excited-state levels, E_{LUMO}s calculated from CV were similar for all the dyes (shown in Table II) and were sufficiently high for electron injection into the TiO_2 (energy level of conducting band is about −4.40 eV). All the present dyes satisfied the energy gap rule. This means that, in thermodynamics, the designed dyes molecules can be used as sensitizers for DSSCs application, in

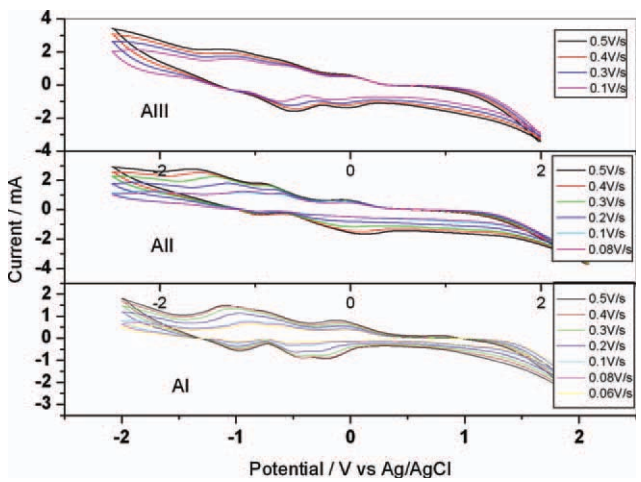

Figure 5 CV curves of AI, AII, and AIII. Scan rates were indicated in labels. [Color figure can be viewed in the online issue, which is available at wileyonlinelibrary.com.]

TABLE II
CV Data of Dyes and Calculated Energy Levels from Experiments and Quantum Chemistry

	E_{red1}/E_{oxd1} (V)[f]	E_{red2}/E_{oxd2} (V)[f]	E_{red} versus Ag/AgCl (V)[b]	E_{Fc} versus Ag/AgCl (V)[c]	E_{red} versus Fc (V)	E_{LUMO} (eV)[d]	E_{HOMO} (eV)[e]	E_g^{opt} (eV)[a]	E_{LUMO} (eV)[g]	E_{HOMO} (eV)[g]	E_g^{opt} (Ev)[a]
AI	−0.2/−0.1	−0.62/−0.57	−0.15	0.64	−0.79	−4.01	−6.29	2.28	−3.60	−5.00	1.40
AII	−0.06/0.14	−0.70/−0.41	0.04	0.64	−0.60	−4.20	−6.46	2.26	$-3.76P^{hP}$	$-4.86P^{hP}$	$1.10P^{gP}$
AIII	−0.03/−0.02	−0.91/−0.15	−0.03	0.64	−0.67	−4.13	−6.40	2.27	–	–	–

[a] Calculated from UV–vis spectra in NMP, $EB_{gPB}^{optP} = 1240/\lambda_{onset}$ (nm). λ_{onset} were estimated from the intercept of the absorption spectra.
[b] $^{P}EB_{red\ vs.\ Ag/AgClPB} = (EB_{red1PB}{}^{+P}EB_{oxd1B})/2$;.
[c] $EB_{Fc\ vs.\ Ag/AgClPB} = (EB_{redPB}{}^{+P}EB_{oxdB})/2 = (0.18 + 1.10)/2 = 0.64$ V;.
[d] Energy level was determined from the formula: E_{LUMO} (eV) $= -|E_A| = -(E_{red} - E_{1/2,ferrocene})$ (eV) + (−4.8) eV.
[e] $EB_{HOMOB}/eV = -|IP| = EB_{LUMOB} - EB_{gPB}^{optP}$.
[f] E versus Ag/AgCl.
[g] Calculated from Gaussian 98 package software through the geometry optimization using DFT method with BPLY6-31 basic.
[h] Values of dimers.

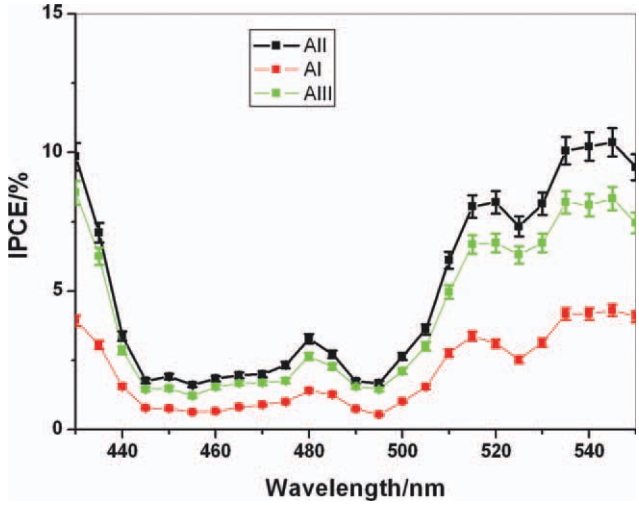

Figure 6 Spectra of monochromatic incident photo-to-current conversion efficiency (IPCE) for DSSC based on A series of compounds in acetonitrile. Every point is representing mean value of three values. [Color figure can be viewed in the online issue, which is available at wileyonlinelibrary.com.]

which the dyes have stronger electron injection driving force.

The kinetics of the perylenediimide-based electrodes can be discussed by looking at the effect of the scan rate on the peak intensity and potential values. It can be seen that the higher the sweep rate values, the higher the peak currents for the film electrodes. At the same time, increasing the scan rate promoted peak broadening and separation, indicating kinetic limitations in the compounds films. These data point to a diffusion-controlled reaction.[34]

Potovoltaic performance of DSSCs based on dyes

The coatings were homogenous and porous with about 40-nm nanocrystalline particle sizes, suitable for the applications in photovolatic devices as shown in Supporting Information Figure S4. The nanocrystalline TiO_2 could adhere to FTO strongly that can not only lower the electron resistance but also adsorb enough dyes to produce photogenerated electrons.

According to the literature,[35] the IPCEs were obtained by the following equation:

$$\mathrm{IPCE}(\%) = \frac{1240 I_{sc}[\mathrm{A/cm^2}] \times 100}{[\lambda(\mathrm{nm}) \times I_{inc}(\mathrm{W/cm^2})]}$$

where I_{sc} is the short-circuit photocurrent density for monochromatic irradiation and λ is the wavelength and I_{inc} is the incident radiative flux.

The IPCE action spectra of the solar cells based on imides and polyimides were shown in Figure 7. AII yielded about 10% at 544 nm. The plots of IPCE

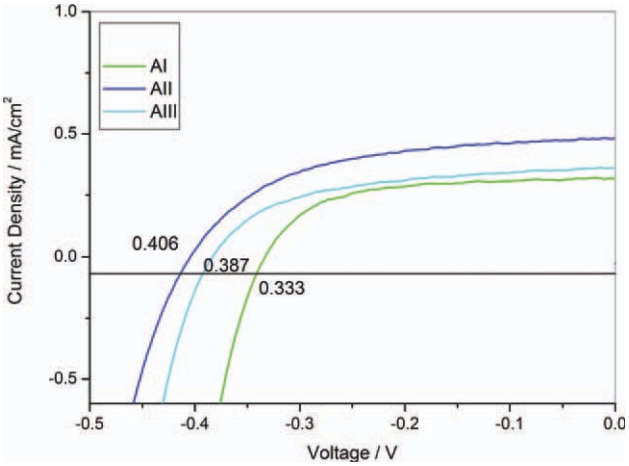

Figure 7 *J–V* characteristics of DSSCs with polyimide and model compounds dyes as sensitizers under illumination of AM 1.5. The effective area: 0.25 cm^2. [Color figure can be viewed in the online issue, which is available at wileyonlinelibrary.com.]

were similar to the UV–vis spectra of polyimides, which indicated that the current originated from the absorption of photon.

The photovoltaic test of DSSCs was carried out by measuring the *J–V* characteristic curves under simulated AM 1.5 solar illumination (90 mW cm^{-2}) in ambient atmosphere (Fig. 7); the fill factor (FF) and overall light-to-electrical energy conversion efficiency (η) of DSSCs were calculated according to the following equation:

$$\eta = \frac{V_{OC} J_{SC} FF}{P_{in}}$$

$$FF = \frac{V_p I_p}{V_{OC} J_{SC}}$$

where J_{SC} is the short-circuit current density (mA cm^{-2}), V_{OC} is the open-circuit voltage (V), P_{in} is the incident light power, and J_p (mA cm^{-2}) and V_p (V) are the current density and voltage at the point of maximum power output on the *J–V* curves, respectively.

From the Figure 7, ηs are in the range of 0.07–0.116%, which are lower than N719. But these values are of the same order of magnitude as some dyes with carboxylic groups reported.[15] It will be full of promise of the dyes after chemical modification.

It has to be noted that for these comparative studies no complete optimization was performed such as modulation of thickness of TiO_2 and adding scattering layer. If optimization of solar cell be carried out, the efficiency would be improved. However, the structure of dye is the key to improve the efficiency. We should design perylene containing dye with carboxyl bonds that would anchor to the TiO_2 surface chemically. The bond would enhance the charges injecting and transferring from dyes to TiO_2. The polyimides are dissolved only in strong polar solvent such as *m*-cresol, DMAc, and NMP. The poor solubility of the polyimide would also decrease the potovoltaic performance of the DSSCs. To avoid the doped of *m*-cresol, we rinsed the dyes and solvent with ethanol and acetonitrile. We also tried to use different solvent to dissolve the dyes, but the photovoltaic results were similar. We need to modify the perylene molecule with some groups such as long alkyl chain to improve the solubility and photovoltaic performance of the polyimides in the future.

Characteristic photocurrents observed on irradiation of electrode under applied biases of −0.4, −0.2, 0, +0.2, and +0.4 V were shown in Figure 8(a). The observed photocurrents increased as the applied potential of the photoelectrochemical cell was shifted to a more positive bias. On illumination under a bias of −0.2 V, a decay of anodic photocurrent and a growth of cathodic current on termination of illumination could be observed. The growth of cathodic current arose from a back electron transfered from reduced TiO_2 nanoparticle to the photooxidized adsorbed dye AIII. The anodic photocurrent under illumination was suppressed at a bias of 0 V and disappeared completely below a bias of −0.4 V. This observation clearly indicated that a positive bias facilitated electron transport across the TiO_2 nanoparticle thin film toward the conducting surface of FTO-coated glass and suppressed the recombination of electrons and holes.

Figure 8(b) showed typical open-circuit photovoltaic response of electrode on illumination at different voltage biases. In contrast to Figure 8(a), the photovoltage did not change as the bias was altered. Photovoltage generation was instantaneous and remained virtually constant over several on-off illumination cycles. This observation was consistent with the injection of electrons from the LUMO of the AIII to the conduction band of the TiO_2 nanoparticles, followed by interparticulate hopping of electrons to the conduction band of the FTO-coated glass. After the light was turned off, the photovoltage decayed to zero instantly.

The *J–V* characteristics of the optimized inverted cell, measured with different incident light intensity from 0 to 90 mW/cm^2, were shown in Supporting Information Figure S6. and data were summarized in Table III. The performance parameters of the cell (J_{sc}) were plotted as functions of the incident light intensities. Because J_{sc} was linear with illuminated light intensity, there was no substantial space charge buildup in the device. The V_{oc} also increased monotonically with an increase of light intensity.

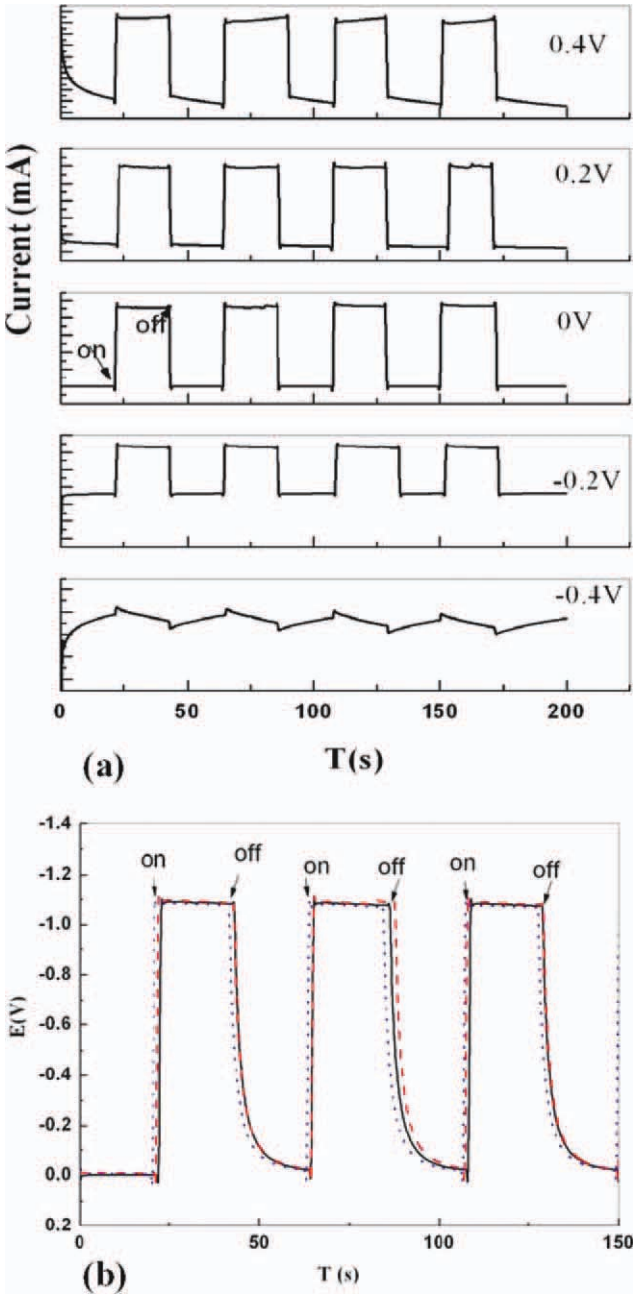

Figure 8 The transient photocurrent response (a) and open-circuit photovoltage (b) of AIII sensitized solar cell at different voltage bias. [Color figure can be viewed in the online issue, which is available at wileyonlinelibrary.com.]

TABLE III
***J–V* Measurement Results of DSSCs Sensitized with AI, AII, AIII, Under Illumination with 90 mW/cm^2 Light Intensity by AM 1.5 Solar Simulator**

	AI	AII	AIII	N719
J_{sc} (mA/cmP^{2P})	0.317	0.526	0.362	14.1
V_{oc} (V)	0.333	0.406	0.387	0.735
PB_{max} (mW/cmP^{2P})	0.063	0.105	0.075	5.35
FF	0.599	0.490	0.534	0.516
η (%)	0.070	0.116	0.083	5.94

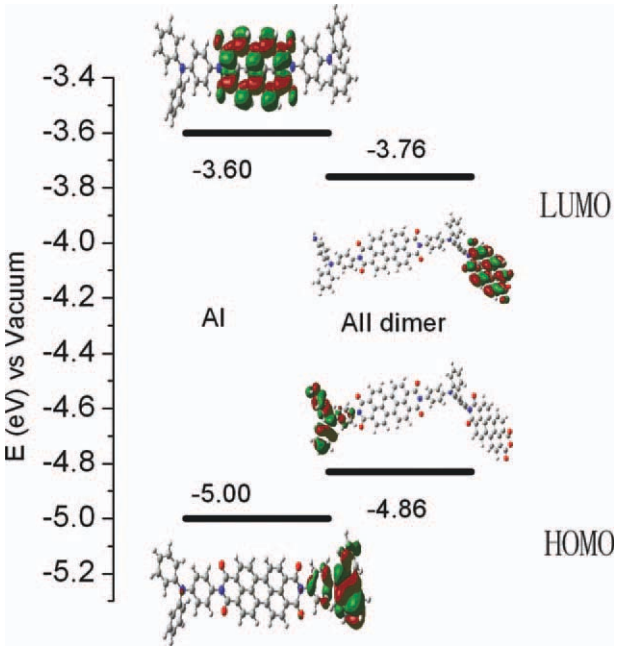

Figure 9 The molecular structures of the novel dyes AI and dimmers of AII and the frontier molecular orbitals calculated with DFT on a B3lYP/6-31G level. [Color figure can be viewed in the online issue, which is available at wileyonlinelibrary.com.]

Electronic structures and molecular simulations

In Figure 9, the structures of the dyes and the Frontier orbitals were depicted by Gaussian software.[17] The diphenylamine moiety was nonplanar and would suppress aggregation due to the disturbance of the π–π stacking. The HOMO was to a large extent distributed over triphenylamine moiety the donor group, and the LUMO was distributed over perylene core plane, which was the acceptor group. The electronic redistribution between the HOMO and LUMO showed a pronounced intramolecular charge separation for this transition. The Frontier molecular orbital energies were summarized in Table II. Because of the computer limit, only energies of dimers of AII were calculated to be compared. With the degree of polymerization increasing and the D-A (donor–acceptor) structure forming, the E_{LUMO}s were decreasing and E_{HOMO}s were increasing that resulted in that the gap between LUMO and HOMO was becoming narrow. Comparison of the electron distribution in the Frontier molecular orbitals revealed that photoinduced electron transfered from the triphenylamine moiety to the perylene moiety. Consequently, electrons could be injected into TiO_2 via the perylene moiety. Assuming similar molecular orbital geometry when molecular anchored to TiO_2, the position of the LUMO close to the anchoring group would enhance the orbital overlap with the titanium 3d orbitals and would favor electron injection.

We also investigated the energy levels of raw monomers of PTDA with same basis level DFT calculations and found that the E_{LUMO}s and E_{HOMO}s were −4.07 and −6.67 eV (not shown here), respectively. When introduced triphenylamine group, the E_{LUMO}s and E_{HOMO}s were improved to provide enough driving force for an efficient electron injection to TiO_2.

There was difference between E_{HOMO}s estimated from CV experiment and DFT free molecule calculations. These can be explained by the nature of the theoretical calculations. The calculations were done for systems with free molecules in a vacuum, but the environment differed substantially from the real experimental conditions, where solvent effects, ions, and molecular interactions play a decisive role in determining the properties.

The molecular aggregation and interaction were also important to the properties of dyes. Looking down the center of the polyimide AII chain in Supporting Information Figure S6, we saw the circle of oxygen and nitrogen. The images showed the folding of the chains. The chains were helicoid, which would suppress aggregation and prevent electron recombination due to the nonplanar conformation of triphenylamine and the disturbance of the π–π stacking. On the one hand, the formed porous centers in the three-dimensional structures would facilitate the ion transport; on the other hand, it would be trouble to transport the electrons along the main molecular chains because of a block of conjugation.

CONCLUSIONS

Three perylene containing dyes were synthesized and the structures were confirmed by ^{1}H-NMR and IR spectra. The optical and photophysical properties were characterized by UV–vis absorption, CV, and quantum chemistry calculation. The three dyes can be dissolved in polar solvents such as NMP and concentrated H_2SO_4. As has been observed with sensitizers adsorbed on nanoporous TiO_2 films, the photosensitization took place by a mechanism involving photoinduced electron injection from the dyes to the TiO_2, and subsequent electron hopping to the conductive FTO electrode surface. Lower efficiencies were observed for the solar cells. It would be explained by some factors such as no chemical bonding to TiO_2, the series resistant of the cell, and the chain conformations. However, the results do demonstrate the viability of polymeric adsorbed photosensitizers for porous nanoparticle metal oxide electrodes and reveal the way of designing of molecules to provide the bright future prospect of developing more efficient DSSCs.

References

1. Nazeeruddin, M. K.; De Angelis, F.; Fantacci, S.; Selloni, A.; Viscardi, G.; Liska, S. P.; Takeru, B.; Grätzel, M. J Am Chem Soc 2005, 127, 16835.
2. Gregg, B. A. J Phys Chem 1996, 100, 852.
3. Hara, K.; Sato, T.; Katoh, R.; Furube, A.; Ohga, Y.; Shinpo, A.; Suga, S.; Sayama, K.; Sugihara, H.; Arakawa, H. J Phys Chem B 2003, 107, 597.
4. Sayama, K.; Tukagoshi, S.; Hara, K.; Ohga, Y.; Shinpo, A.; Abe, Y. J Phys Chem B 2002, 106, 1363.
5. Hara, K.; Kurashige, M.; Dan, Y.; Kasada, C.; Shinpo, A.; Saga, S. New J Chem 2003, 27, 783.
6. Tokuhisa, H.; Hammond, P. T. Adv Funct Mater 2003, 13, 831.
7. Horiuchi, T.; Miura, H.; Uchida, S. J Am Chem Soc 2004, 126, 12218.
8. Mende, L. S.; Fechtenkötter, A.; Müllen, K.; Moons, E.; Friend, R. H.; MacKenzie, J. D. Science 2001, 293, 1119.
9. O'Neil, M. P.; Niemczyk, M. P.; Sves, W. A.; Gosztola, D.; Gaines, G. L.; Wasielewski, M. R. Science 1992, 257, 63.
10. Langhals, H.; Jona, W. Angew Chem Int Ed Engl 1998, 37, 952.
11. Ferrere, S.; Gregg, B. New J Chem 2002, 26, 1155.
12. Tian, H.; Liu, P.; Zhu, W.; Gao, E.; Wu, D.; Cai S. J Mater Chem 2000, 10, 2708.
13. Jin, Y.; Hua, J.; Wu, W.; Ma, X.; Meng, F. Synth Metals 2008, 158, 64.
14. Ferrere, S.; Gregg, B. A. J Phys Chem B 2001, 105, 7602.
15. Zafer, C.; Kus, M.; Turkmen, G.; Dincalp, H.; Demic, S.; Kuban, B.; Teoman, Y.; Icli, S. Solar Energ Mater Solar Cells 2007, 91, 427.
16. Zhang, X.; Wu, Y.; Li, J.; Li, F.; Li, M. Dyes Pigments 2008, 76, 810.
17. Fortage, J.; Séverac, M.; Houarner-Rassin, C.; Pellegrin, Y.; Blart, E.; Odobel, F. J Photochem Photobiol A: Chem 2008, 197, 156.
18. Erten, S.; Alp, S.; Icli, S. J Photochem Photobiol A: Chem 2005, 175, 214.
19. Mackinnon Sean, M.; Wang, Z. Y. J Polym Sci A: Polym Chem 2000, 38, 3467.
20. Shibano, Y.; Umeyama, T.; Matano, Y.; Imahori, H. Org Lett 2007, 9, 1971.
21. Li, C.; Pschirer, N.; Schneboom, J.; Eickemeyer, F.; Sens, R.; Boschloo, G.; Herrmann, A.; Mllen, K.; Hagfeldt, A.; Edvinsson, T. J Phys Chem C 2007, 111, 15137.
22. Li, G.; Jiang, K.; Li, Y.; Li, S.; Yang, L. J Phys Chem C 2008, 112, 11591.
23. Ning, Z.; Zhang, Q.; Wu, W.; Pei, H.; Liu, B.; Tian, H. J Org Chem 2008, 73, 3791.
24. Liang, M.; Xu, W.; Cai, F.; Chen, P.; Peng, B.; Chen, J.; Li, Z. J Phys Chem C 2007, 111, 4465.
25. Hagher, D. P.; Edvinsson, T.; Marinado, T.; Boschloo, G.; Hagfeldt, A.; Sun, L. Chem Commun 2006,2245.
26. Cha, C. S.; Yang, H. X. J Power Sources 1993, 43, 145.
27. Frisch, M. J.; Trucks, G. W.; Schlegel, H. B.; Scuseria, G. E.; Robb, M. A.; Cheeseman, J. R.; Zakrzewski, V. G.; Montgomery, J. A., Jr.; Stratmann, R. E.; Burant, J. C.; Dapprich, S.; Millam, J. M.; Daniels, A. D.; Kudin, K. N.; Strain, M. C.; Farkas, O.; Tomasi, J.; Barone, V.; Cossi, M.; Cammi, R.; Mennucci, B.; Pomelli, C.; Adamo, C.; Clifford, S.; Ochterski, J.; Petersson, G. A.; Ayala, P. Y.; Cui, Q.; Morokuma, K.; Malick, D. K.; Rabuck, A. D.; Raghavachari, K.; Foresman, J. B.; Cioslowski, J.; Ortiz, J. V.; Baboul, A. G.; Stefanov, B. B.; Liu, G.; Liashenko, A.; Piskorz, P.; Komaromi, I.; Gomperts, R.; Martin, R. L.; Fox, D. J.; Keith, T.; Al-Laham, M. A.; Peng, C. Y.; Nanayakkara, A.; Challacombe, M.; Gill, P. M. W.; Johnson, B.; Chen, W.; Wong, M. W.; Andres, J. L.; Gonzalez, C.;

Head-Gordon, M.; Replogle, E. S.; Pople, J. A. Gaussian 98, Gaussian, Inc.: Pittsburgh, PA, 1998.
28. Chiu, K. Y.; Su, T. X.; Li, J. H.; Lin, T.; Liou, G. S.; Cheng, S. H. J Electroanal Chem 2005, 575, 95.
29. Meng, X.; Huang, Y.; Niu, H.; Lei, Z. Chinese J Org Chem 2007, 27, 682.
30. Fang, J.; Kita, H.; Okamoto, K. Macromolecules 2000, 33, 4639.
31. Wang, Z. Y.; Qi, Y.; Gao, J. P.; Sacrpante, G. G.; Sundararajan, P. R.; Duff, J. D. Macromolecules 1998, 31, 2075.
32. Schouwink, P.; Schafer, A. H.; Seidel, C.; Fuchs, H. Thin Solid Films 2000, 372, 163.
33. Seybold, G.; Wagenblast, G. Dyes Pigments 1989, 4, 303.
34. Parra, V.; Del Cano, T.; Rodríguez-Méndez, M. L.; de Saja, J. A.; Aroca, R. F. Chem Mater 2004, 16, 358.
35. Kamat, P. V. J Phys Chem C 2007, 111, 2834.